ADVANCED QUANTUM TECHNOLOGIES
www.advquantumtech.com

Bi-Frequency Illumination: A Quantum-Enhanced Protocol

Mateo Casariego, Yasser Omar, and Mikel Sanz*

Quantum-enhanced, idler-free sensing protocol to measure the response of a target object to the frequency of a probe in a noisy and lossy scenario is proposed. In this protocol, a target with frequency-dependent reflectivity $\eta(\omega)$ embedded in a thermal bath is considered. The aim is to estimate the parameter $\lambda = \eta(\omega_2) - \eta(\omega_1)$, since it contains relevant information for different problems. For this, a bi-frequency quantum state is employed as the resource, since it is necessary to capture the relevant information about the parameter. Computing the quantum Fisher information H relative to the parameter λ in an assumed neighborhood of $\lambda \approx 0$ for a two-mode squeezed state (H_Q), and a pair of coherent states (H_C), a quantum enhancement is shown in the estimation of λ. This quantum enhancement grows with the mean reflectivity of the probed object, and is noise-resilient. Explicit formulas are derived for the optimal observables, and an experimental scheme based on elementary quantum optical transformations is proposed. Furthermore, this work opens the way to applications in both radar and medical imaging, in particular in the microwave domain.

1. Introduction

Quantum information technologies are opening very promising prospects for faster computation, securer communications, and more precise detection and measuring systems, surpassing the capabilities and limits of classical information technologies.[1–5] Namely, in the domain of quantum sensing and metrology,[6] we are currently witnessing a boost of applications to a wide spectrum of physical problems: from gravimetry and geodesy,[7–11] gravitational waves,[12] clock synchronization,[5,13] thermometry[14] and bio-sensors,[15–19] to experimental proposals to seek quantum behavior in macroscopic gravity,[20] to name just a few.

While many of the quantum metrology studies that focus on unlossy and noiseless (unitary) scenarios, the more realistic, lossy case has also been investigated.[21–29] Equivalently, one can talk about quantum metrology with open quantum systems. Understanding what are the precision limits of measurements in the presence of loss is a fundamental endeavor in quantum metrology.[30,31] Certain noise properties have been found to be beneficial in some scenarios,[32,33] and quantum error correction schemes have been proposed to overcome decoherence and restore the quantum-enhancement.[34] Quantum illumination (QI)[35–45] is a particularly interesting example of a lossy and noisy protocol where the use of entanglement proves useful even in an entanglement-breaking scenario. QI shows that the detection of a low-reflectivity object in a noisy thermal environment with a low-intensity signal is enhanced when the signal is entangled to an idler that is kept for a future joint measurement with the reflected state. This makes QI a candidate for a quantum radar,[46] although a more involved protocol is needed.[47,48] The decision problem of whether there is an object or not can be rephrased as a quantum estimation of the object's reflectivity

M. Casariego, Y. Omar
Instituto Superior Técnico
Universidade de Lisboa
Portugal
E-mail: mateo.casariego@tecnico.ulisboa.pt

M. Casariego, Y. Omar
Physics of Information and Quantum Technologies Group
Centro de Física e Engenharia de Materiais Avançados (CeFEMA)
Portugal

Y. Omar
PQI – Portuguese Quantum Institute
Portugal

M. Sanz
Department of Physical Chemistry
University of the Basque Country UPV/EHU
Apartado 644, Bilbao E-48080, Spain

M. Sanz
EHU Quantum Center
University of the Basque Country UPV/EHU

M. Sanz
Basque Center for Applied Mathematics (BCAM)
Alameda de Mazarredo 14, Bilbao, Basque Country 48009, Spain

M. Sanz
IKERBASQUE
Basque Foundation for Science
Plaza Euskadi 5, Bilbao 48009, Spain

The ORCID identification number(s) for the author(s) of this article can be found under https://doi.org/10.1002/qute.202100051

DOI: 10.1002/qute.202100051

η, in order to discriminate an absence ($\eta = 0$) from a presence ($\eta \ll 1$) of a low-reflectivity object.[49]

The goal of quantum estimation[50–54] is to construct an estimator $\tilde{\lambda}$ for certain parameter λ characterizing the system. It is noteworthy that not every parameter in a system corresponds to an observable, and this may imply the need for data post-processing. Either way, the theory provides techniques to obtain an optimal observable—not necessarily unique, that is, whose mean square error is minimal. The estimator $\tilde{\lambda}$ is nothing but a map from the results of measuring the optimal observable to the set of possible values of the parameter λ. One of the main results of this theory is the quantum Cramér–Rao (qCR) bound, which sets the ultimate precision of any estimator. Whether this bound is achievable or not depends on the data-analysis method used, and on the statistical distribution of the outcomes of different runs of the experiment. In most practical situations, maximum likelihood methods for unbiased estimators, together with a Gaussian distribution of the outcomes of the (independent) runs of the experiment, make the bound achievable. In order to find the qCR—and the explicit form of the optimal observable—one needs to compute the quantum Fisher information[55] (QFI), which roughly speaking quantifies how much information about λ can be extracted from the system, provided that an optimal measurement is performed. In general, computing the QFI involves diagonalization of the density matrix, which makes the obtention of analytical results challenging. However, if one restricts to Gaussian states and Gaussian-preserving operations,[56–59] the so-called symplectic approach simplifies the task considerably.[60–70] As the QFI is by definition optimized over all POVMs, it only depends on the initial state, often called *probe*. This means that a second optimization of the QFI can be pursued, this time over all possible probes. Moreover, this approach allows us to quantitatively compare different protocols, for example, with and without entanglement in the probe, since an increase in the QFI when the same resources are used—which typically translates into fixing the particle number, or the energy—directly means an improvement in precision.

In this article, we propose an idler-free quantum-enhanced, lossy protocol to estimate the reflectivity $\eta(\omega)$ of an object as a function of the frequency when the object is embedded in a noisy environment. In particular, we propose a method where a bi-frequency state is sent to probe a target—modeled as a beam splitter with a frequency-dependent reflectivity $\eta(\omega)$ and embedded in a thermal environment. The goal is to obtain an estimator for the parameter $\lambda = \eta(\omega_2) - \eta(\omega_1)$, that captures information about the linear frequency dependence of the object. For simplicity, it is assumed that the frequencies are sufficiently close so that we can work in a neighborhood of $\lambda \approx 0$.

By imposing that the expected photon number is the same in quantum and classical scenarios, we find the QFI ratio between them, and analyze when it is greater than one. We find that the maximum enhancement is obtained for highly reflective targets, and derive explicit limits in the highly noisy case. We also provide expressions for the optimal observables, proposing a general experimental scheme described in Figure 2, and motivating applications in microwave technology.[71]

The article is structured as follows. First, we introduce the model, along with the main concepts and formulas from quantum estimation theory, motivating the use of Gaussian states. Then, we compute the QFI and show the quantum enhancement. Finally, we compute the optimal observables for both the quantum and the classical probes, and briefly discuss applications.

2. Model and Fundamentals of Quantum Estimation Theory with Gaussian States

2.1. Physics of Gaussian States

When a quantum system has one or more degree of freedom described by operators with a continuous spectrum, we say that the system is a “continuous variable” (CV) system. Within the bosonic CV quantum systems, quantum Gaussian states are defined as the ones arising from Hamiltonians that are at most quadratic in the field operators, which we list in the vector $\hat{\boldsymbol{A}} := (\hat{a}_1, \hat{a}_2, \dots, \hat{a}_N, \hat{a}_1^\dagger, \hat{a}_2^\dagger, \dots \hat{a}_N^\dagger)$, where N is the number of modes. This ordering of the creation and annihilation operators is commonly referred to as the “complex basis” or “complex form,”[57] and allows for a compact way of writing down the commutation relations: $[\hat{A}_a, \hat{A}_b] = K_{ab}\hat{\mathrm{I}}$, where $a, b = 1, \dots, N$, $\hat{\mathrm{I}}$ is the identity operator, and $K = \mathrm{diag}(\mathbb{1}_N, -\mathbb{1}_N)$ is a diagonal matrix, $\mathbb{1}_N$ being the $N \times N$ identity matrix.

Instead of having to resort to the infinite-dimensional density operator in order to describe a state, Gaussian systems are fully characterized by an N-vector called the *displacement vector* and an $N \times N$ matrix, the *covariance matrix*. We can construct the displacement vector

$$\boldsymbol{d} := \mathrm{Tr}\left[\rho \hat{\boldsymbol{A}}\right] \tag{1}$$

and the covariance matrix

$$\Sigma := \mathrm{Tr}\left[\rho \{\Delta\hat{\boldsymbol{A}}, \Delta\hat{\boldsymbol{A}}^{\intercal}\}\right] \tag{2}$$

where ρ is the density operator, $\{\cdot,\cdot\}$ denotes the anticommutator, and $\Delta\hat{\boldsymbol{A}} := \hat{\boldsymbol{A}} - \boldsymbol{d}$. It is important to bear in mind that other choices of basis lead to different, but equivalent definitions. In fact, in the following sections we will start by writing down covariance matrices in the so-called “quadrature basis” $(\hat{x}_1, \dots, \hat{x}_N, \hat{p}_1, \dots, \hat{p}_N)$ with the *canonical* position and momentum operators defined by the choice $\kappa_1 = 2^{-1/2}$ in $\hat{a}_k = \kappa_1(\hat{x}_k + i\hat{p}_k)$.[72] A key result with important consequences in the context of Gaussian states is the normal mode decomposition,[73,74] which follows the more general theorem due to Williamson[75] and that, from a physical point of view, establishes that any Gaussian Hamiltonian (i.e., quadratic) is equivalent —up to a unitary— to a set of free, non-coupled harmonic oscillators. This apparent simplicity of Gaussian states, however, has a rich structure when it comes to analyzing their Hilbert space properties, as well as information-theoretic quantities such as the quantum Fisher information, entropies, and so on. We can state the result in the following way: any positive-definite Hermitian matrix Σ of size $2N \times 2N$ can be diagonalized with a symplectic matrix S: $\Sigma = SDS^\dagger$, where $D = \mathrm{diag}(\nu_1, \dots, \nu_N, \nu_1, \dots, \nu_N)$ with ν_a the symplectic eigenvalues of Σ, that are the positive eigenvalues of matrix $K\Sigma$. An important result for what follows is that a state is pure if and only if all the symplectic eigenvalues are one: $\nu_a = 1$ $\forall a$, and $\nu_a \geq 1$ for any Gaussian state.

2.2. Quantum Estimation

Quantum metrology is so related to quantum estimation that sometimes the two terms are used as synonyms. Incidentally, quantum sensing could be seen as a quantum estimation or metrology problem that deals with a binary question: is the value of the parameter of interest zero or not? Terminology aside, quantum estimation deals with the problem of measuring things that may not be encoded in observables per se, that is, it allows for the obtention of measurable quantities that do not necessarily correspond to linear functions of the density matrix, and it teaches us what the ultimate precision limits are, whether one can attain them or not, and how to attain them. The most common approach to attack the problem of metrology is from the notion of classical *frequentist* estimation. Although the –perhaps more realistic– approach of Bayesian quantum estimation theory[76–82] exists and is a rich field of research, here we will take the former, tacitly assuming a *local* estimation strategy,[83,84] that happens when there is some prior knowledge of the interval where the true value of the parameter (or parameters) of interest may lie, hence its name: the true parameter value is localized into some interval rather than completely unknown (in this case, the estimation is called *global*). In the local approach, the QFI matrix emerges as the figure of merit for the quantification of the maximum amount of information one can extract from the system.

While classical parameter estimation deals only with the statistics of measurement outcomes, and answers questions of attainability in the presence of statistical noise (with various properties that can affect the scaling of the precision with which one estimates the parameter), quantum estimation addresses the problem of *what* to measure, and imposes additional limits to the precision due to the fundamental probabilistic nature of quantum mechanics. Indeed, the quantum Fisher information (QFI) matrix, can be seen as an optimization of the classical Fisher information—a measure for the amount of information relative to a set of parameters λ a system contains—over all possible measurements, or POVMs.

The QFI can be interpreted geometrically by means of a notion of distance in the Hilbert space spanned by density operators. Among the many candidates, the Bures distance

$$D_{\mathrm{B}}^2(\rho_1,\rho_2) := 2\left(1-\sqrt{F(\rho_1,\rho_2)}\right) \tag{3}$$

where $F(\rho_1,\rho_2) := (\mathrm{Tr}[\sqrt{\sqrt{\rho_1}\rho_2\sqrt{\rho_1}}])^2$ is the Uhlmann fidelity between states ρ_1 and ρ_2, the one correctly linking estimation to geometry. This makes the interpretation of quantum estimation straightforward: it depends upon the distinguishability between states. If λ is a vector of parameters that defines a (possibly continuous) family of states $\{\rho_\lambda\}$, then the Bures distance between two infinitesimally close states can be related to a metric tensor, which is no other than the QFI matrix:

$$D_{\mathrm{B}}^2(\rho_\lambda,\rho_{\lambda+\mathrm{d}\lambda}) = \frac{H_{ab}(\lambda)}{4} \tag{4}$$

A large QFI translates in a large distinguishability between states. In this paper we will focus on the single parameter case, for which the QFI is a scalar that can be computed using the following basis-dependent formula

$$H(\lambda) = 2\sum_{m,n}\frac{|\langle\Phi_m|\,\partial_\lambda\rho_\lambda\,|\Phi_n\rangle|^2}{\rho_m+\rho_n} \tag{5}$$

where $\{\rho_m, |\Phi_m\rangle\}$ are the eigensolutions to $\rho_\lambda|\Phi_m\rangle = \rho_m|\Phi_m\rangle$, and ρ_λ is the measured, or received state. Moreover, the theory also provides a way of finding an optimal observable, whose outcomes allow us to construct an estimator:[53]

$$\hat{O}_\lambda = \lambda\mathbb{1} + \frac{\hat{L}_\lambda}{H(\lambda)} \tag{6}$$

where $\hat{L}_\lambda$ is a symmetric logarithmic derivative (SLD) that solves the equation $\{\hat{L}_\lambda,\rho_\lambda\} = 2\partial_\lambda\rho_\lambda$, where $\{\cdot,\cdot\}$ is the anticommutator. When the estimator $\tilde{\lambda}$ is constructed using a maximum likelihood method, the so-called quantum Cramér–Rao bound (qCRB)[85,86] is asymptotically achieved, meaning that the observable in Equation (6) has the smallest possible variance:

$$\mathrm{var}(\hat{O}_\lambda) \geq \frac{1}{MH(\lambda)} \tag{7}$$

where $\mathrm{var}(\hat{O}) := \langle\hat{O}^2\rangle - \langle\hat{O}\rangle^2$ denotes the variance of operator $\hat{O}$, M is the number of repetitions, and $H(\lambda)$ is the QFI.

The problem, however, can become mathematically challenging due to the diagonalization implicit in Equation (5). In the next section we review some results that help us circumvent these issues, as long as we stick to Gaussian states.

2.2.1. Gaussian Quantum Estimation

As shown in ref. [60], when we are in the presence of Gaussian states and Gaussian-preserving channels, there is no need to diagonalize the density matrix in Equation (5) in order to find the QFI. For a single parameter, the QFI can be computed using

$$\begin{aligned}H(\lambda) = \frac{1}{2(\det[A]-1)}\Bigg[&\det[A]\,\mathrm{Tr}\left[(A^{-1}\partial_\lambda A)^2\right] \\ &+ \sqrt{\det[\mathbb{1}_2 + A^2]}\,\mathrm{Tr}\left[\left((\mathbb{1}_2+A^2)^{-1}\partial_\lambda A\right)^2\right] \\ &- 4\left(\nu_+^2-\nu_-^2\right)\left(\frac{(\partial_\lambda\nu_+)^2}{\nu_+^4-1} - \frac{(\partial_\lambda\nu_-)^2}{\nu_-^4-1}\right)\Bigg] + 2\partial_\lambda\boldsymbol{d}^\dagger\Sigma_\lambda^{-1}\partial_\lambda\boldsymbol{d}\end{aligned} \tag{8}$$

where the *dot* over A and $\vec{d}$ denotes derivative with respect to λ, and $\nu_\pm$ are the *symplectic eigenvalues* of Σ_λ, defined following ref. [61]

$$2\nu_\pm^2 := \mathrm{Tr}[A^2] \pm \sqrt{(\mathrm{Tr}[A^2])^2 - 16\det[A]} \tag{9}$$

with the matrix A given by $A := i\Omega T\Sigma_\lambda T^\intercal$, $\Omega := \mathrm{antidiag}(\mathbb{1}_2, -\mathbb{1}_2)$, and $T_{ij} := \delta_{j+4,2i} + \delta_{j,2i-1}$ is the matrix that changes the basis to the *quadrature basis*$(\hat{x}_1^{\mathrm{th}}, \hat{x}_1^{\mathrm{S}}, \hat{x}_2^{\mathrm{th}}, \hat{x}_2^{\mathrm{S}}, \hat{p}_1^{\mathrm{th}}, \hat{p}_1^{\mathrm{S}}, \hat{p}_2^{\mathrm{th}}, \hat{p}_2^{\mathrm{S}})^\intercal$. For a Gaussian

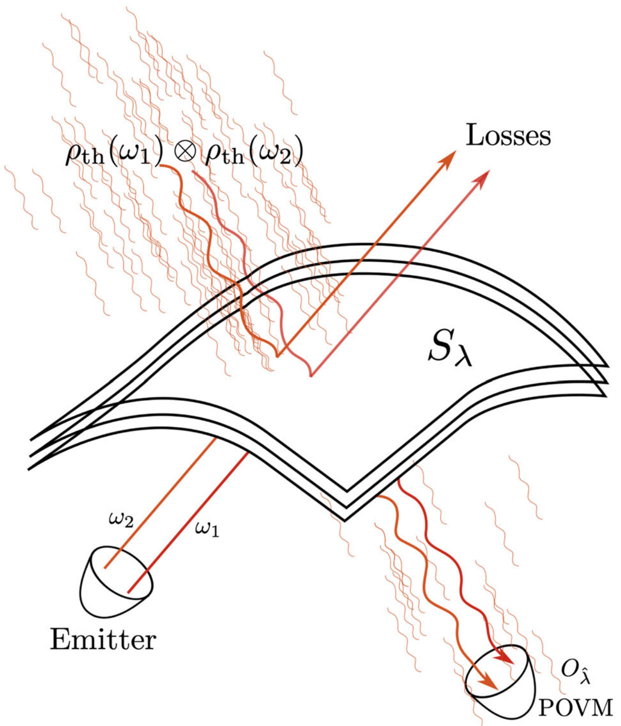

Figure 1. An object reflects a bi-frequency beam (notice the similar but different colors of the two beams coming out of the emitter), and mixes it with a thermal bath for each frequency with the same expected photon number, coming from the upper left. The transmitted signal and reflected thermal state are lost, and a measurement $O_{\hat{\lambda}}$ is performed onto the available part (lower right corner), whose expectation values converge, after classical data processing, to an estimator of the parameter λ encoded in the object. In our case, S_λ represents the transformation associated to a multi-layered object, modeled as a beam splitter, where $\lambda := \eta_2 - \eta_1$ is the parameter to be estimated, where $\eta_i = \eta(\omega_i)$ are the reflectivities for the different frequencies. The emitter can produce either a pair of coherent states (classical strategy) or an entangled, two-mode squeezed state. The latter proves advantageous in the parameter estimation, giving a strictly larger quantum Fisher information.

state $(\Sigma_\lambda, \vec{d}_\lambda)$ written in the complex basis, the symmetric logarithmic derivative in Equation (6) can be obtained as in ref. [60]:

$$\hat{L}_\lambda = \Delta\vec{\hat{A}}^\dagger \mathcal{A}_\lambda \Delta\vec{\hat{A}} - \mathrm{Tr}[\Sigma_\lambda \mathcal{A}_\lambda]/2 + 2\Delta\vec{\hat{A}}^\dagger \Sigma_\lambda^{-1}\partial_\lambda \vec{d}_\lambda \tag{10}$$

where $\Delta\vec{\hat{A}} := \vec{\hat{A}} - \vec{d}_\lambda$, $\vec{\hat{A}}$ the *complex basis* vector of bosonic operators, $\mathcal{A}_\lambda := \mathcal{M}^{-1}\partial_\lambda \vec{d}_\lambda$, where $\mathcal{M} = \bar{\Sigma}_\lambda \otimes \Sigma_\lambda - K \otimes K$, where the bar denotes complex conjugate, and $K := \mathrm{diag}(\mathbb{1}_2, -\mathbb{1}_2)$. Note that when $\lambda \to 0$ we have $\hat{O}_{\lambda=0} \equiv \hat{O} = \hat{L}_{\lambda=0}/H(\lambda=0)$, since both limits exist independently. This limit is of our interest because we will work in a neighborhood of $\lambda \approx 0$, that is, the measured value of the parameter is expected to be small (i.e. we shall adopt a local estimation strategy).

2.3. Model

The model is synthesized in **Figure 1**, the target object, modeled as a beam splitter with a frequency-dependent reflectivity is subject to an illumination with a bi-frequency probe. The transmitted signal is lost, and only the reflected part is collected for measurement. For a single frequency, a beam splitter is characterized by a unitary operator

$$U(\omega) \equiv \exp\left[\arcsin\left(\sqrt{\eta(\omega)}\right)\left(\hat{s}_\omega^\dagger \hat{b}_\omega e^{i\varphi} - \hat{s}_\omega \hat{b}_\omega^\dagger e^{-i\varphi}\right)\right] \tag{11}$$

where $\eta(\omega)$ is a frequency-dependent reflectivity, related to transmittivity τ via $\eta(\omega) + \tau(\omega) = 1$.

We assume for simplicity that $\varphi = 0$, that is, there is no phase difference between transmitted and reflected signals. This unitary maps states (density matrices) that live in the density matrix space associated with Hilbert space $\mathcal{H}$, $\mathcal{D}(\mathcal{H})$ to itself. Formulating the problem from a density operator perspective, we have that the received state is

$$\rho_\lambda = \mathrm{Tr}_{S_1}\mathrm{Tr}_{S_2}\left[U_\lambda \rho U_\lambda^\dagger\right] \tag{12}$$

where the parameter is defined as $\lambda = \eta(\omega_2) - \eta(\omega_1)$, and $\rho \in \mathcal{H}_{S_1,S_2,B_1,B_2}$ is a four-mode state that includes the two signals (the two-mode state that we can control) and two thermal environments of the form $\rho_1^{\rm th} \otimes \rho_2^{\rm th}$, where the subscript indicates the frequency, that is, $\rho_a^{\rm th} = (1+N_{\rm th})^{-1}\sum_{n=0}^\infty (N_{\rm th}/(1+N_{\rm th}))^n |n\rangle_a \langle n|$ where $N_{\rm th} = \mathrm{Tr}(\rho_a^{th}\hat{b}_{\omega_a}^\dagger \hat{b}_{\omega_a})$ is the average number of thermal photons, which we assume to be the same for the two modes. Note that in order to obtain the explicit form of the interaction U_λ in Equation (12) one just needs to reparametrize the four-mode unitary $U(\omega_1) \otimes U(\omega_2)$ using the difference of reflectivities $\lambda \equiv \eta_2 - \eta_1$ and Equation (11). The equal thermal photon number is an accurate approximation as long as the frequency difference $\Delta\omega \equiv \omega_2 - \omega_1$ is sufficiently small. To make this statement more quantitative, let us assume two different thermal photon densities, N_1 and N_2. The Bose–Einstein distribution for photons is $N_i \propto 1/(e^{\beta\omega_i} - 1)$ where $\beta \equiv \hbar/k_{\rm B}T$ is a function of the temperature T. Then,

$$\frac{N_1}{N_2} = \frac{e^{\beta\omega_1} - 1}{e^{\beta\omega_2} - 1} = \frac{1}{1 + \frac{\beta\Delta\omega e^{\beta\omega_1}}{e^{\beta\omega_1} - 1}} \tag{13}$$

we see that up to first order in $\beta\Delta\omega$, the last expression reduces to $1 - \Delta\omega/\omega_1$. This means that $N_1 \approx N_2$ if $\Delta\omega/\omega_1 \ll 1$. In particular, for $T = 300$ K and $\omega_1/2\pi = 5$ GHz the expected thermal photon number is roughly 1250. It is straightforward to check that for these frequencies and temperatures, the above approximations are good (that is, $\approx 4\%$ of relative error) for frequency differences up to 20%.

Because we are working within the local estimation approach and our goal is to find observables that saturate the qCRB, we shall take the true value of λ to be exactly zero. This means that the goal of the protocol is to increase one's confidence about this initial ansatz of the parameter being zero, and be able to tell when it is close but not exactly zero. Hence, we work in a neighborhood of $\lambda \approx 0$—which can be implemented by taking the limit $\lambda \to 0$ in the derived expressions. Moreover, this relies on a physical assumption, since we are interested in probing regions of $\eta(\omega)$ that do not change drastically, that are well approximated by a linear function with either no slope or a small one. In this sense, the protocol is a quantum sensing one, since we are interested in answering the question of whether the parameter either vanishes or is small.

It is also worth discussing briefly the effect of absorption loss due to the medium through which the signal travels. These can be accommodated in the model by means of an additional beam splitter. The medium through which the signal travels can be seen as an array of infinitesimal beam splitters, each of which having the same reflectivity, and mixing some incoming signal with the same thermal state. For a travel distance L, the flying mode will see a reflectivity

$$\eta_{\text{abs}} = 1 - e^{-\mu L} \tag{14}$$

where μ is a parameter characterizing the photon-loss of the medium. A concatenation of beam splitters can be easily put into a single one, as long as they are embedded in the same environment, which is our case. For beam splitters of transmittivities τ_1 and τ_2 their combined resulting transmittivity is simply the product: $\tau = \tau_1\tau_2$. Thus, accommodating absorption losses into our model is trivially obtained by the transformation $\tau \mapsto e^{-\mu L}\tau$. Since the QFI deals with derivatives with respect to the parameter to be estimated, and ultimately we are interested in QFI *ratios* between a quantum protocol and its classical counterpart, the above transformation will not affect the overall results, since multiplicative factors will cancel out.

3. Results: Quantum Fisher Information

In this section we compute the QFI for two different probes: an entangled two-mode squeezed (TMS) state, and a pair of coherent beams. The choice of the TMS state over other possible entangled states is motivated by the fact that these are customarily produced in labs, both in optical -for example, with non-linear crystals, and in microwave frequencies—using Josephson parametric amplifiers (JPAs).

3.1. Two-Mode Squeezed Vacuum State

The TMS vacuum (TMSV) state is the continuous-variable equivalent of the Bell state, being the Gaussian state that optimally transforms classical resources (light, or photons) into quantum correlations. The TMSV state is a cornerstone in experiments with quantum microwaves.[87–91] In our case, we are interested in states produced via nondegenerate parametric amplification, in order to have two distinguishable frequencies. The state can be formally written as: $|\psi\rangle_{\text{TMSV}} := (\cosh r)^{-1}\sum_{n=0}^{\infty}(-e^{i\phi}\tanh r)^n\,|n,n\rangle$, where $r \in \mathbb{R}_{\geq 0}$ is the *squeezing parameter*. For simplicity we take $\phi = 0$. In any realistic application, the TMSV state should be replaced by a TMS thermal state, which can be defined as the one obtained by applying the two-mode squeezing operation to a pair of uncorrelated thermal states $\rho_{\text{th},1}$, and $\rho_{\text{th},2}$ with mean thermal photon numbers n_1 and n_2, respectively, and hence resulting in a mixed state.[92] The expected total photon number in these states is given by $N_{\text{TMST}} = \langle \hat{N}_1 + \hat{N}_2\rangle = (n_1+n_2)\cosh 2r + 2\sinh^2 r$, where $\hat{N}_i \equiv \hat{a}^{\dagger}_{S_i}\hat{a}_{S_i}$ for $i = 1, 2$. Typically, one has $n_1 = n_2 \equiv n$, which gives us a symmetric TMST state. In this case we define the signal photon number N_{S} as the photon number in each of the modes, $N_{\text{S}} \equiv N_{\text{TMST}}/2 = n(1+2N_r) + N_r$, where $N_r \equiv \sinh^2 r$.[93,94] In microwaves, a squeezing level $S = -10\log_{10}[(1+2n)\exp(-2r)]$ of 9.1 dB has been reported[95] for $n = 0.34$ and $r \approx 1.3$, using JPAs operating at roughly 5 GHz with a filter bandwidth of 430 kHz. This corresponds to $N_{\text{S}} \approx 8$.

The total initial (real) covariance matrix –written in the *real basis* $(\hat{x}_1^{\text{th}}, \hat{p}_1^{\text{th}}, \hat{x}_1^{\text{S}}, \hat{p}_1^{\text{S}}, \hat{x}_2^{\text{th}}, \hat{p}_2^{\text{th}}, \hat{x}_2^{\text{S}}, \hat{p}_2^{\text{S}})^{\intercal}$– is given by

$$\Sigma = N\begin{pmatrix} N^{-1}\Sigma_{\text{th}} & 0 & 0 & 0 \\ 0 & \Sigma_r & 0 & \varepsilon_r \\ 0 & 0 & N^{-1}\Sigma_{\text{th}} & 0 \\ 0 & \varepsilon_r^{\intercal} & 0 & \Sigma_r \end{pmatrix} \tag{15}$$

where $N \equiv 1 + 2n$, $\Sigma_{\text{th}} = (1 + 2N_{\text{th}})\mathbb{1}_2$ is the real covariance matrix of a thermal state, $\Sigma_r = \cosh(2r)\mathbb{1}_2$ corresponds to the diagonal part of one of the modes in a TMSV state, and $\varepsilon_r = \sinh(2r)\sigma_Z$ is the correlation between the two modes, where σ_Z is the Z Pauli matrix. Note that the covariance matrix of the thermal TMS state is simply N times the one of the TMSV state.

The displacement vector of a TMST state is identically zero $\boldsymbol{d}_{\text{TMST}} = \boldsymbol{0}$, so the last term of Equation (8) vanishes. Under the assumption that the object does not entangle the two modes, we have that the symplectic transformation is $S(\eta_1,\eta_2) = S_{\text{BS}}(\eta_1) \oplus S_{\text{BS}}(\eta_2)$,[96] where

$$S_{\text{BS}}(x) = \begin{pmatrix} \sqrt{x}\mathbb{1}_2 & \sqrt{1-x}\mathbb{1}_2 \\ -\sqrt{1-x}\mathbb{1}_2 & \sqrt{x}\mathbb{1}_2 \end{pmatrix} \tag{16}$$

is the real symplectic transformation associated with a beam splitter of reflectivity x. We define the parameter of interest as $\lambda \equiv \eta_2 - \eta_1$. With this, $S(\eta_1,\eta_2)$ becomes a function of λ. For simplicity, we define $S_\lambda := S(\eta_1, \eta_1 + \lambda)$. The full state after the signals get mixed with the thermal noise is given by $\tilde{\Sigma}_\lambda \equiv S_\lambda \Sigma S_\lambda^{\intercal}$. In covariance matrix formalism, partial traces are implemented by removing the corresponding rows and columns;[57] in our case the rows and columns 1, 2, 5, and 6. The resulting *received* covariance matrix reads as follows

$$\Sigma_\lambda = \begin{pmatrix} a\mathbb{1} & b\sigma_Z \\ b\sigma_Z & c\mathbb{1} \end{pmatrix} \tag{17}$$

with $a \equiv 1 + 2N_{\text{th}} + 2\eta_1(2N_r + 4nN_r - N_{\text{th}})$, $b \equiv 2(1+2n)\sqrt{2\eta_1 N_{\text{S}}(\eta_1+\lambda)(2N_{\text{r}}+1)}$, and $c \equiv (1+2n)(1+4\lambda N_r + \eta_1(4N_r - 2N_{\text{th}}) + 2(1-\lambda)N_{\text{th}})$.

For this state, the symplectic eigenvalues $\nu_\pm$ defined in Equation (9) are strictly larger than one for any value of the parameters n, N_r, N_{th}, and η_1, other than $\eta_1 = 1 \wedge N_{\text{th}} = 0$, so there is no need of any regularization scheme.[61] Indeed, this is due to the mixedness of the received state: regularization is only needed for pure states.

We obtain the function $H_{\text{Q}}(\lambda)$ from Equation (8), and compute the two-sided limit $H_{\text{Q}} \equiv \lim_{\lambda\to 0} H_{\text{Q}}(\lambda)$ when the parameter

λ goes to zero, finding

$$H_{\mathrm{Q}} = \kappa\big[\eta_1\bar{n}\left(\bar{N}_{\mathrm{th}}(4nN_r + n + 4N_r - 2N_{\mathrm{th}}) - 2\eta_1(2(n+1)N_r\bar{N}_{\mathrm{th}} + N_{\mathrm{th}}(n - N_{\mathrm{th}}))\right) + \beta\big)\big(\eta_1\bar{n}\left(\bar{N}_{\mathrm{th}}(4nN_r + n + 4N_r - 2N_{\mathrm{th}}) - 2\eta_1(2(n+1)N_r\bar{N}_{\mathrm{th}} + N_{\mathrm{th}}(n - N_{\mathrm{th}}))\right) + \beta + 1\big] \tag{18}$$

where

$$\kappa^{-1} \equiv \bar{n}^2\big[2\eta_1(\bar{N}_{\mathrm{th}}(N_r(\bar{n}(8(n+1)N_r^2 + 6nN_r + n) - 4N_r) + 2N_{\mathrm{th}}^2(4nN_r + n + 6N_r) - 2N_rN_{\mathrm{th}}(2(6n+5)N_r + 2n - 1) - 2N_{\mathrm{th}}^3) - 2\eta_1(-N_{\mathrm{th}}(4(n+1)N_r + n) + N_r((4n+2)N_r - 1) + N_{\mathrm{th}}^2)(2(n+1)N_r\bar{N}_{\mathrm{th}} + N_{\mathrm{th}}(n - N_{\mathrm{th}}))) + 2n(2N_r + 1)N_r\bar{N}_{\mathrm{th}}^2 + 4N_r^2(6N_{\mathrm{th}}(N_{\mathrm{th}} + 1) + 1) - 4N_rN_{\mathrm{th}}^2(4N_{\mathrm{th}} + 3) + N_{\mathrm{th}}^2\bar{N}_{\mathrm{th}}^2\big] \tag{19}$$

and $\bar{N}_{\mathrm{th}} \equiv 1 + 2N_{\mathrm{th}}$, $\bar{n} \equiv 1 + 2n$, and $\beta \equiv n\bar{N}_{\mathrm{th}}^2 + 2N_{\mathrm{th}}(N_{\mathrm{th}} + 1)$.

3.2. Coherent States

Here we use a pair of coherent states as probe: $|\psi\rangle = |\alpha\rangle \otimes |\alpha\rangle$. The total expected photon number in this state is $2N_{\mathrm{C}} := 2|\alpha^2|$. For simplicity we take $\alpha \in \mathbb{R}$. Moreover, since we will compare with the TMST state, we set $\alpha^2 = n(1 + 2N_r) + N_r$. The initial covariance matrix is simply given by the direct sum of two identity matrices (corresponding to each of the coherent states), and two thermal states. After the interaction and the losses, the measured covariance matrix is

$$\Sigma_\lambda = \begin{pmatrix} d\mathbb{1} & 0 \\ 0 & f\mathbb{1} \end{pmatrix} \tag{20}$$

where $d = 1 + 2N_{\mathrm{th}}\tau_1, f = 1 + 2N_{\mathrm{th}}(\tau_1 - \lambda)$.

The initial displacement vector in the real basis is $\boldsymbol{d}_0^{\intercal} = (0, 0, \sqrt{2}\alpha, 0, 0, 0, \sqrt{2}\alpha, 0)$ which leads—after the interaction and the trace of the losses—to $\boldsymbol{d}^{\intercal} = \alpha(\sqrt{2\eta_1}, 0, \sqrt{2(\eta_1 + \lambda)})$. The symplectic eigenvalues are also larger than one here. Inserting these in Equation (8), and taking the limit $\lambda \to 0$, we find that the QFI for the coherent state is

$$H_{\mathrm{C}} = \frac{4N_{\mathrm{th}}^2\left((1 + 2N_{\mathrm{th}}\tau_1)^2 + 1\right)}{(1 + 2N_{\mathrm{th}}\tau_1)^4 - 1} + \frac{n(1 + 2N_r) + N_r}{\eta_1(1 + 2N_{\mathrm{th}}\tau_1)} \tag{21}$$

where $\tau_1 = 1 - \eta_1$ is the transmittivity. Having computed both the quantum and the classical QFIs, in the next section we analyze their ratio $H_{\mathrm{Q}}/H_{\mathrm{C}}$, a quantifier for the quantum enhancement.

3.3. Comparison: Quantum Enhancement

We analyze the ratio between the TMST state's QFI (H_{Q}) and the coherent pair's QFI (H_{C}) for different situations. As a first approximation and to simplify the discussion, we take the limit where $n \to 0$, which corresponds to a TMSV state input. Finding values of $(\eta_1, N_{\mathrm{th}}, N_{\mathrm{S}})$ such that the ratio $H_{\mathrm{Q}}/H_{\mathrm{C}}$ is larger than one means that one can extract more information about parameter λ using a TMST state than using a coherent pair, provided an optimal measurement is performed in both cases. In **Figure 2** we plot the results for various values of η_1. We can immediately see that the ratio gets larger for large values of η_1, that is, for highly reflective materials. In particular, we find the high-reflectivity limit the ratio converges even when the individual QFIs do not (since they correspond to a pure state being transmitted):

$$\lim_{\eta_1\to 1}\frac{H_{\mathrm{Q}}}{H_{\mathrm{C}}} = \frac{N_{\mathrm{S}}^2\left(8N_{\mathrm{th}}(N_{\mathrm{th}} + 1) + 4\right) + 4N_{\mathrm{S}}N_{\mathrm{th}}^2 + N_{\mathrm{th}}^2}{N_{\mathrm{th}}\left(N_{\mathrm{S}}(4N_{\mathrm{th}} + 2) + N_{\mathrm{th}}\right)} \tag{22}$$

which converges to $1 + 8N_{\mathrm{S}}^2/(4N_{\mathrm{S}} + 1)$ in the highly noisy scenario $N_{\mathrm{th}} \gg 1$. Using a squeezing of $r \approx 1.3$ which is experimentally realistic for microwave quantum states, and that corresponds to an expected photon number of $N_{\mathrm{S}} \approx 2.9$, we expect to find a quantum-enhancement of roughly a factor of six, that is, $H_{\mathrm{Q}}/H_{\mathrm{C}} \approx 6.4$ in the highly reflective limit.

In the next section we explicitly compute the observables that lead to an optimal extraction of λ's value for both the classical and the quantum probes.

4. Optimal Observables

Here we address the question of how to extract the maximum information about parameter λ for each of the probes. The theory provides us with explicit ways to compute an optimal POVM, which albeit not unique, provides us with an optimal measurement strategy: upon measuring the outcomes and possibly after some classical data-processing, the results asymptotically tend toward the true value of the parameter to be estimated.

4.1. Optimal Observable for the TMSV State Probe

Computing the SLD in Equation (8) and inserting it in Equation (6) we find

$$\hat{O}_{\mathrm{Q}} = L_{11}\hat{a}_1^\dagger\hat{a}_1 + L_{22}\hat{a}_2^\dagger\hat{a}_2 + L_{12}\left(\hat{a}_1^\dagger\hat{a}_2^\dagger + \hat{a}_1\hat{a}_2\right) + L_0\mathbb{1}_{12} \tag{23}$$

where the general expressions for the coefficients can be found in Appendix A. The variance of this operator is found to be $\mathrm{var}(\hat{O}_{\mathrm{Q}}) = 2N_{\mathrm{S}}^2L_{12}(1 + N_{\mathrm{S}})$. We can numerically test the validity of the qCR bound for this observable by examining the bound itself for the extreme choice of $M = 1$. The saturation of the bound produces the following relation:

$$\mathrm{var}\left(\hat{O}_{\mathrm{Q}}\right)H_{\mathrm{Q}} = 1 \tag{24}$$

Now, as the left hand side a function of $(N_{\mathrm{S}}, N_{\mathrm{th}}, \eta_1)$, we can give different values to the reflectivity and find the limiting condition between N_{S} and N_{th}, which is depicted in **Figure 3**. Naturally, the larger M, the better results we can achieve, but $M = 1$ proves the existence of a choice of parameters for which the bound is saturated.

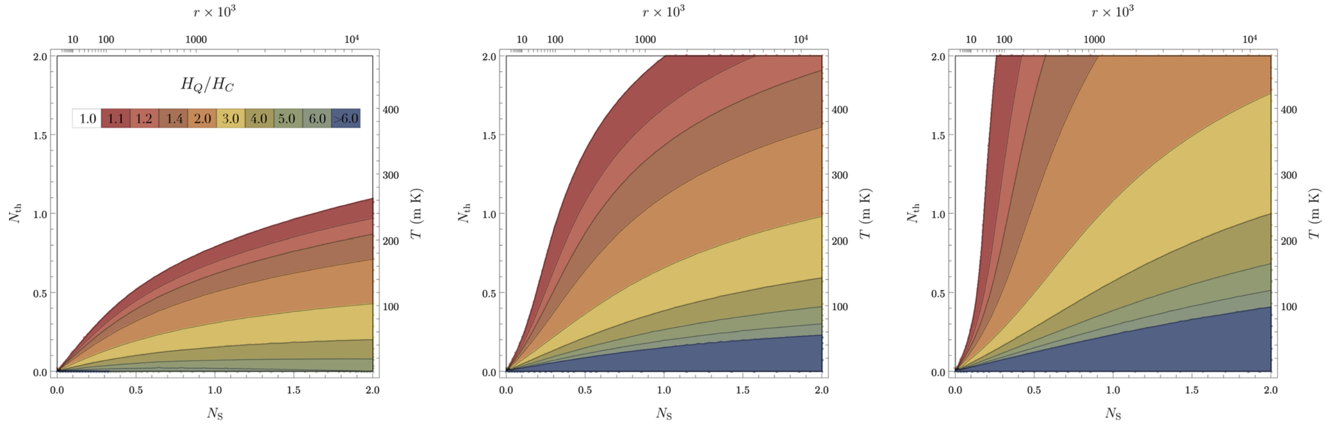

a) $\eta_1 = 0.75$ b) $\eta_1 = 0.90$ c) $\eta_1 = 0.95$

Figure 2. Values, represented by a non-linear color grading, of the quantum enhancement given by the ratio H_Q/H_C of the quantum Fisher information of the two-mode squeezed vacuum state probe H_Q by the quantum Fisher information of the coherent states probe H_Q as a function of the photon numbers of the signal (N_S) and of the thermal bath (N_{th}), for a reflectivity η_1 of a) 0.75, b) 0.90, and c) 0.95. Equivalently, scales of squeezing, r, given by $\sqrt{N_S} = \sinh r$, and temperature T in Kelvin, are provided. The relation between temperature and mean thermal photon number is obtained via the usual Bose–Einstein distribution $N_{th} = 1/(\exp(E/k_B T) - 1)$ when the energy is set to $E = \hbar\omega = h\nu$, which requires a choice of the frequency ν. We have taken $\nu = 5$ GHz, a typical frequency of microwaves. White represents no quantum enhancement, that is, $H_Q/H_C = 1$. We clearly see that as η_1 grows, the quantum enhancement becomes not only more significant, but also easier to achieve with less signal photons. Importantly, as the reference reflectivity η_1 grows, the protocol becomes more resilient to thermal noise.

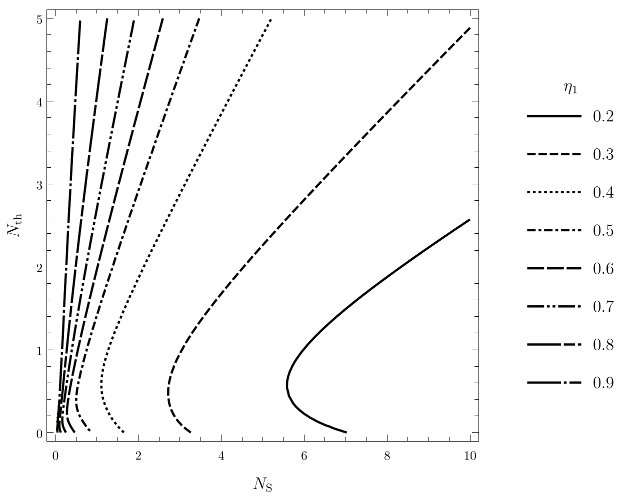

Figure 3. Proof of the saturation of the quantum Cramér–Rao bound for the optimal observable $\hat{O}_Q$ given in Equation (23) for different values of the reflectivity η_1, expressed as the existence of a real function $N_{th} = N_{th}(N_S)$, for the extreme case of just one experimental run ($M = 1$). As the reflectivity grows, we observe an interesting behavior: the best choice of N_{th}—defined as the one that saturates the bound while keeping N_S as low as possible—is actually non-vanishing.

Moreover, it is illustrative to study a possible implementation of the noiseless case, since this captures the essence of what is being measured. When $N_{th} \to 0$ we have that $\hat{O}_Q^{\text{Lim}} = -\mu^2 \hat{a}_1^\dagger \hat{a}_1 - \hat{a}_2^\dagger \hat{a}_2 + \mu(\hat{a}_1^\dagger \hat{a}_2^\dagger + \hat{a}_1 \hat{a}_2) - \nu \mathbb{1}_{12}$ where $\mu^2 \equiv (1 + 1/2N_S)$ and $\nu \equiv (1 + 1/4N_S)$, and we have taken the limit of vanishing N_{th}. Notice that we can rewrite this observable as $\hat{b}_1^\dagger \hat{b}_1 - 1$, that is, implementing photon-counting on the operator $\hat{b}_1 \equiv -i(\hat{a}_2^\dagger - \mu \hat{a}_1)$. This is achieved by means of the transformations captured in **Figure 4**.

Following that scheme, we have that after the first beam splitter

$$
\begin{aligned}
\hat{a}_1' &= \hat{a}_1 \cos\varphi + \hat{a}_2 \sin\varphi \\
\hat{a}_2' &= -\hat{a}_1 \sin\varphi + \hat{a}_2 \cos\varphi
\end{aligned}
\tag{25}
$$

then the Josephson parametric amplifiers (JPA)—-ideally squeezing operators—produce $\hat{a}_i'' = S^\dagger(r_i, \theta_i)\hat{a}_i' S(r_i, \theta_i)$ where $S(r_i, \theta_i)$ is the squeezing operator, acting as

$$
\begin{aligned}
\hat{a}_i'' &= S^\dagger(r_i, \theta_i)\hat{a}_i' S(r_i, \theta_i) = \hat{a}_i' \cosh r_i - e^{i\theta_i} \hat{a}_i'^\dagger \sinh r_i \\
\hat{a}_i''^\dagger &= S^\dagger(r_i, \theta_i)\hat{a}_i'^\dagger S(r_i, \theta_i) = \hat{a}_i'^\dagger \cosh r_i - e^{-i\theta_i} \hat{a}_i' \sinh r_i.
\end{aligned}
\tag{26}
$$

Assuming that the phase shifter ϕ acts as $\hat{c} \mapsto e^{-i\phi}\hat{c}$ we find the following output modes

$$
\begin{aligned}
e^{i\phi}\hat{b}_1 &= \cos\theta\left(\hat{a}_1' \cosh r_1 - e^{i\theta_1} \hat{a}_1'^\dagger \sinh r_1\right) + \sin\theta\left(\hat{a}_2' \cosh r_2 - e^{i\theta_2} \hat{a}_2'^\dagger \sinh r_2\right) \\
\hat{b}_2 &= -\sin\theta\left(\hat{a}_1' \cosh r_1 - e^{i\theta_1} \hat{a}_1'^\dagger \sinh r_1\right) + \cos\theta\left(\hat{a}_2' \cosh r_2 - e^{i\theta_2} \hat{a}_2'^\dagger \sinh r_2\right).
\end{aligned}
\tag{27}
$$

We insert Equation (25) in the last expression and regroup, finding

$$
\begin{aligned}
e^{i\phi}\hat{b}_1 = {} & \hat{a}_1\left(\cos\theta \cos\varphi \cosh r_1 - \sin\theta \sin\varphi \cosh r_2\right) \\
& + \hat{a}_2\left(\cos\theta \sin\varphi \cosh r_1 + \sin\theta \cos\varphi \cosh r_2\right) \\
& + \hat{a}_1^\dagger\left(-e^{i\theta_1} \cos\theta \cos\varphi \sinh r_1 + e^{i\theta_2} \sin\theta \sin\varphi \sinh r_2\right) \\
& + \hat{a}_2^\dagger\left(-e^{i\theta_1} \cos\theta \sin\varphi \sinh r_1 - e^{i\theta_2} \sin\theta \cos\varphi \sinh r_2\right)
\end{aligned}
\tag{28}
$$

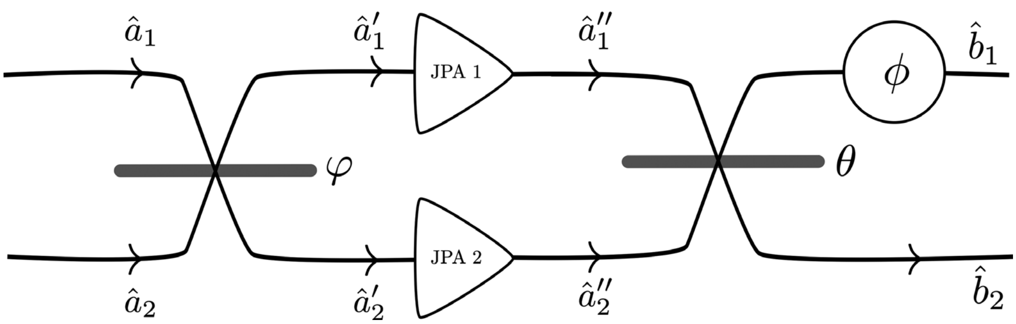

Figure 4. Schematic circuit for the generation of mode $\hat{b}_1$, needed to correctly implement the optimal observable in the two-mode squeezed vacuum (TMSV) state. The original $\hat{a}_i$ modes mix at a φ beam splitter, and the outputs go through a single-mode squeezing operator—Josephson parametric amplifier (JPA) in microwaves, with parameters r_i and θ_i corresponding to squeezing and phase. Then they mix at a second beam splitter θ. A phase shift ϕ is applied at the end, to cancel undesired terms. This scheme is technology-independent, and could be applied to optics by replacing the JPAs with the corresponding squeezing device, for example, a non-linear crystal that performs spontaneous parametric down-conversion.

Because we want to perform photon-counting over the operator $\hat{b}_1 \equiv -i(\hat{a}_2^\dagger - \mu\hat{a}_1)$, we identify:

$$i\mu = \cos\theta\cos\varphi\cosh r_1 - \sin\theta\sin\varphi\cosh r_2 \tag{29}$$

$$i = e^{i\theta_1}\cos\theta\sin\varphi\sinh r_1 + e^{i\theta_2}\sin\theta\cos\varphi\sinh r_2. \tag{30}$$

4.2. Optimal Observable for the Coherent State Probe

The optimal observable in this case is given by $\hat{O}_C = A\mathbb{1}_{(1)} \otimes [(\hat{a}_2^\dagger - \eta_1\sqrt{\alpha})(\hat{a}_2 - \eta_1\sqrt{\alpha}) + \frac{1}{2}]$, where $A = 1/(\eta_1 - 1)(1 - N_{\text{th}}(\eta_1 - 1))$, and $\mathbb{1}_{(1)}$ is the absence of active measurement of mode 1. This expression can then be put as $\hat{O}_C = A\mathbb{1}_{(1)} \otimes [(\hat{a}_2^\dagger - \eta_1\sqrt{\alpha})(\hat{a}_2 - \eta_1\sqrt{\alpha}) + \frac{1}{2}]$. This operator can be experimentally performed with a displacement $D(-\eta_1\sqrt{\alpha})$[97] and photon-counting in the resulting mode. The interpretation is simple: because η_1 is known (it serves as a reference), there is nothing to be gained by measuring the first mode in the absence of entanglement. Moreover, the observable is separable, as one should expect, and the experimental implementation is straightforward: photon-counting in the—locally displaced—second mode.

We have seen that both quantum and classical observables are non-Gaussian measurements, since they can be related to photon-counting, as expected in order to obtain quantum enhancement.[59] Current photon counters in microwave technologies can resolve up to three photons with an efficiency of 96%.[98] Inefficiencies in the photon-counters can be accounted for with a simple model of an additional beam splitter that mixes the signal with either a vacuum or a low-temperature thermal state. Additionally, the fact that real digital filters are not perfectly sharp should also be accounted for in a full experimental proposal, which we leave for future work.[99]

5. Conclusions

We have proposed a novel protocol for achieving a quantum enhancement in the decision problem of whether a target's reflectivity depends or not on the frequency, using a bi-frequency, entangled probe, in the presence of noise and losses. Crucially, our protocol needs no idler mode, avoiding the necessity of coherently storing a quantum state in a memory. The scaling of the quantum Fisher information (QFI) associated to the estimation problem for the entangled probe is faster than in the case of a coherent signal. This quantum enhancement is more significant in the high reflectivity regime. Moreover, we have derived analytic expressions for the optimal observables, which allow extraction of the maximum available information about the parameter of interest, sketching an implementation with quantum microwaves.

This information can be related to the electromagnetic response of a reflective object to changes in frequency, and, consequently, the protocol can be applied to a wide spectrum of situations. Although the results are general, we suggest two applications within quantum microwave technology: radar physics, motivated by the atmospheric transparency window in the microwaves regime, together with the naturally noisy character of open-air;[71,98,100–103] and quantum-enhanced microwave medical contrast-imaging of low penetration depth tissues, motivated not only by the non-ionizing nature of these frequencies, but also because resorting to methods that increase the precision and/or resolution without increasing the intensity of radiation is crucial in order not to heat the sample.

Our work paves the way for extensions of the protocol to accommodate both thermal effects in the input modes, and continuous-variable frequency entanglement,[104] where a more realistic model for a beam containing a given distribution of frequencies could be used instead of sharp, ideal bi-frequency states. It also serves as reminder that quantum enhancement provided by entanglement can survive noisy, lossy channels.

Appendix A: Coefficients for the Optimal Quantum Observable

Here we give the general expressions of the coefficients of the optimal observable for the TMS state:

$$\hat{O}_Q = L_{11}\hat{a}_1^\dagger\hat{a}_1 + L_{22}\hat{a}_2^\dagger\hat{a}_2 + L_{12}\left(\hat{a}_1^\dagger\hat{a}_2^\dagger + \hat{a}_1\hat{a}_2\right) + L_0\mathbb{1}_{12} \tag{A1}$$

$$
\begin{aligned}
L11 &= -\frac{2\eta_1 N_S(2N_S+1)(2N_{th}+1)}{-A+B-C+D} \\
L22 &= \frac{4\eta_1(2\eta_1-1)N_S^2(2N_{th}+1)+2N_S(\eta_1-2N_{th}((\eta_1-3)\eta_1+(\eta_1-1)(3\eta_1-1)N_{th}+1)-1)+N_{th}(2(\eta_1-1)N_{th}((\eta_1-1)N_{th}-1)+1)}{A-B+C-D} \\
L12 &= -\frac{\sqrt{2}\sqrt{N_S(2N_S+1)}\left(\eta_1^2\left(N_S(4N_{th}+2)-N_{th}^2\right)+N_{th}(N_{th}+1)\right)}{A-B+C-D} \\
L_0 &= -\frac{4\eta_1^3\left(N_{th}^2-2N_S(2N_{th}+1)\right)^2-2\eta_1^2(6N_{th}+5)F\left(N_S(4N_{th}+2)-N_{th}^2\right)+4\eta_1(N_{th}+1)\left(N_S^2(8N_{th}+4)-2N_S(N_{th}(6N_{th}+5)+1)+N_{th}^2(3N_{th}+2)\right)+(2N_{th}+3)GF}{E-4\eta_1(2N_{th}+1)F\left(-4N_SN_{th}+N_S(2N_S-1)+N_{th}^2\right)-8N_S^2(3N_{th}(N_{th}+1)+1)+4N_SN_{th}(N_{th}(4N_{th}+3)+1)-2N_{th}^2G}
\end{aligned}
\tag{A2}
$$

where

$$
\begin{aligned}
A &\equiv 8(\eta_1-1)\eta_1 N_S^3(2N_{th}+1) \\
B &\equiv 4N_S^2\left(-\eta_1+(\eta_1+3\eta_1N_{th})^2-\eta_1N_{th}(10N_{th}+7)+3N_{th}(N_{th}+1)+1\right) \\
C &\equiv 2N_SN_{th}(-\eta_1+N_{th}(\eta_1(3\eta_1-8)+4(\eta_1-1)(2\eta_1-1)N_{th}+3)+1) \\
D &\equiv N_{th}^2(2(\eta_1-1)N_{th}((\eta_1-1)N_{th}-1)+1) \\
E &\equiv 4\eta_1^2\left(-4N_SN_{th}+N_S(2N_S-1)+N_{th}^2\right)\left(N_S(4N_{th}+2)-N_{th}^2\right) \\
F &\equiv 2N_S-N_{th} \\
G &\equiv 2N_{th}(N_{th}+1)+1
\end{aligned}
\tag{A3}
$$

In the high reflectivity case $\eta_1 \to 1$ we find:

$$
\begin{aligned}
\lim_{\eta_1\to1} L_{11} &= -\frac{2N_S(2N_S+1)(2N_{th}+1)}{N_S^2(8N_{th}(N_{th}+1)+4)+4N_SN_{th}^2+N_{th}^2} \\
\lim_{\eta_1\to1} L_{22} &= -\frac{4N_S(2N_SN_{th}+N_S+N_{th})+N_{th}}{N_S^2(8N_{th}(N_{th}+1)+4)+4N_SN_{th}^2+N_{th}^2} \\
\lim_{\eta_1\to1} L_{12} &= \frac{2\sqrt{2}\sqrt{N_S(2N_S+1)}(N_S(4N_{th}+2)+N_{th})}{N_S^2(8N_{th}(N_{th}+1)+4)+4N_SN_{th}^2+N_{th}^2} \\
\lim_{\eta_1\to1} L_0 &= \frac{-2N_S(N_S(8N_{th}+4)+6N_{th}+1)-3N_{th}}{8N_S^2(2N_{th}(N_{th}+1)+1)+8N_SN_{th}^2+2N_{th}^2}
\end{aligned}
\tag{A4}
$$

Additionally, as shown in the main text, in the noiseless case we get

$$
\begin{aligned}
\hat{O}_Q^{\text{Lim}} := \lim_{\substack{N_{th}\to0\\ \eta_1\to1}} \hat{O}_Q &= -\mu^2\hat{a}_1^\dagger\hat{a}_1-\hat{a}_2^\dagger\hat{a}_2+\mu\left(\hat{a}_1^\dagger\hat{a}_2^\dagger+\hat{a}_1\hat{a}_2\right)-\nu\mathbb{1}_{12} \\
&\equiv \hat{b}_1^\dagger\hat{b}_1-1
\end{aligned}
\tag{A5}
$$

where $\mu^2 \equiv (1+1/2N_S)$ and $\nu \equiv (1+1/4N_S)$ and $\hat{b}_1 \equiv -i(\hat{a}_2^\dagger-\mu\hat{a}_1)$.

Acknowledgements

The authors acknowledge the support from the EU H2020 Quantum Flagship project QMiCS (820505). M.C. acknowledges support from the DP-PMI and FCT (Portugal) through scholarship PD/BD/135186/2017. M.C. and Y.O. thank the support from Fundação para a Ciência e a Tecnologia (Portugal), namely through the project UIDB/04540/2020, as well as from project TheBlinQC supported by the EU H2020 QuantERA ERA-NET cofunded by Quantum Technologies and by FCT (QuantERA/0001/2017). M.S. acknowledge financial support from Basque Government QUANTEK project from ELKARTEK program (KK-2021/00070) and the Basque Government project IT1470-22, Spanish Ramón y Cajal Grant RYC-2020-030503-I and the project grant PID2021-125823NA-I00 funded by MCIN/AEI/10.13039/501100011033 and by "ERDF A way of making Europe" and "ERDF Invest in your Future," as well as from OpenSuperQ (820363) of the EU Flagship on Quantum Technologies, and the EU FET-Open projects Quromorphic (828826) and EPIQUS (899368).

Conflict of Interest

The authors declare no conflict of interest.

Data Availability Statement

The data that support the findings of this study are available from the corresponding author upon reasonable request.

Keywords

entanglement, quantum advantage, quantum enhancement, quantum illumination, quantum microwaves, quantum parameter estimation, quantum sensing

Received: March 30, 2021
Revised: September 6, 2022
Published online: October 13, 2022

[1] M. A. Nielsen, I. L. Chuang, *Quantum Computation and Quantum Information: 10th Anniversary Edition*, Cambridge University Press, Cambridge **2010**.
[2] F. Arute, K. Arya, R. Babbush, D. Bacon, J. C. Bardin, R. Barends, R. Biswas, S. Boixo, F. G. S. L. Brandao, D. A. Buell, B. Burkett, Y. Chen, Z. Chen, B. Chiaro, R. Collins, W. Courtney, A. Dunsworth, E. Farhi, B. Foxen, A. Fowler, C. Gidney, M. Giustina, R. Graff, K. Guerin, S. Habegger, M. P. Harrigan, M. J. Hartmann, A. Ho, M. Hoffmann, T. Huang, et al., *Nature* **2019**, *574*, 505.
[3] S. L. Braunstein, *Phys. Rev. Lett.* **1992**, *69*, 3598.

[4] S. Pirandola, B. R. Bardhan, T. Gehring, C. Weedbrook, S. Lloyd, *Nat. Photonics* **2018**, *12*, 724.
[5] H. Katori, *Nat. Photonics* **2011**, *5*, 203.
[6] V. Giovannetti, S. Lloyd, L. Maccone, *Nat. Photonics* **2011**, *5*, 222.
[7] K. Bongs, Y. Singh, *Nat. Photonics* **2020**, *14*, 408.
[8] V. Ménoret, P. Vermeulen, N. Le Moigne, S. Bonvalot, P. Bouyer, A. Landragin, B. Desruelle, *Sci. Rep.* **2018**, *8*, 12300.
[9] J. Flury, *J. Phys.: Conf. Ser.* **2016**, *723*, 012051.
[10] J. Grotti, S. Koller, S. Vogt, S. Häfner, U. Sterr, C. Lisdat, H. Denker, C. Voigt, L. Timmen, A. Rolland, F. N. Baynes, H. S. Margolis, M. Zampaolo, P. Thoumany, M. Pizzocaro, B. Rauf, F. Bregolin, A. Tampellini, P. Barbieri, M. Zucco, G. A. Costanzo, C. Clivati, F. Levi, D. Calonico, *Nat. Phys.* **2018**, *14*, 437.
[11] E. Zeuthen, E. S. Polzik, F. Ya. Khalili, *Phys. Rev. D* **2019**, *100*, 062004.
[12] J. Aasi, J. Abadie, B. Abbott, R. Abbott, T. D. Abbott, M. R. Abernathy, C. Adams, T. Adams, P. Addesso, R. X. Adhikari, C. Affeldt, O. D. Aguiar, P. Ajith, B. Allen, E. Amador Ceron, D. Amariutei, S. B. Anderson, W. G. Anderson, K. Arai, M. C. Araya, C. Arceneaux, S. Ast, S. M. Aston, D. Atkinson, P. Aufmuth, C. Aulbert, L. Austin, B. E. Aylott, S. Babak, P. T. Baker, et al., *Nat. Photonics* **2013**, *7*, 613.
[13] E. O. Ilo-Okeke, L. Tessler, J. P. Dowling, T. Byrnes, *npj Quantum Inf.* **2018**, *4*, 40.
[14] A. De Pasquale, T. M. Stace, in *Thermodynamics in the Quantum Regime* (Eds: F. Binder, L. Correa, C. Gogolin, J. Anders, G. Adesso), Fundamental Theories of Physics, Vol. *195*, Springer, Cham **2018**.
[15] M. Taylor, J. Janousek, V. Daria, J. Knittel, B. Hage, H.-A. Bachor, W. P. Bowen, *Nat. Photonics* **2013**, *7*, 229.
[16] M. H. Mohammady, H. Choi, M. E. Trusheim, A. Bayat, D. Englund, Y. Omar, *Phys. Rev. A* **2018**, *97*, 042124.
[17] J. Cai, F. Jelezko, M. B. Plenio, *Nat. Commun.* **2014**, *5*, 4065.
[18] F. Dolde, H. Fedder, M. W. Doherty, T. Nöbauer, F. Rempp, G. Balasubramanian, T. Wolf, F. Reinhard, L. C. L. Hollenberg, F. Jelezko, J. Wrachtrup, *Nat. Phys.* **2011**, *7*, 459.
[19] K. Jensen, R. Budvytyte, R. A. Thomas, T. Wang, A. M. Fuchs, M. V. Balabas, Ge. Vasilakis, L. D. Mosgaard, H. C. Stærkind, J. H. Müller, T. Heimburg, S.-P. Olesen, E. S. Polzik, *Sci. Rep.* **2016**, *6*, 29638.
[20] S. Bose, A. Mazumdar, G. W. Morley, H. Ulbricht, M. Toroš, M. Paternostro, A. A. Geraci, P. F. Barker, M. S. Kim, G. Milburn, *Phys. Rev. Lett.* **2017**, *119*, 240401.
[21] S. Lee, Y. S. Ihn, Z. Kim, *Phys. Rev. A* **2020**, *101*, 012332.
[22] C. Oh, S. Lee, H. Nha, H. Jeong, *Phys. Rev. A* **2017**, *96*, 062304.
[23] X. Zhang, Y. Yang, X. Wang, *Phys. Rev. A* **2013**, *88*, 013838.
[24] Y. M. Zhang, X. W. Li, W. Yang, G. R. Jin, *Phys. Rev. A* **2013**, *88*, 043832.
[25] R. Demkowicz-Dobrzański, J. Kołodyński, M. Guţă, *Nat. Commun.* **2012**, *3*, 1063.
[26] B. M. Escher, L. Davidovich, N. Zagury, R. L. de Matos Filho, *Phys. Rev. Lett.* **2012**, *109*, 190404.
[27] R. Chaves, J. B. Brask, M. Markiewicz, J. Kołodyński, A. Acín, *Phys. Rev. Lett.* **2013**, *111*, 120401.
[28] P. Sekatski, M. Skotiniotis, W. Dür, *New J. Phys.* **2016**, *18*, 073034.
[29] P. Sekatski, M. Skotiniotis, J. Kołodyński, W. Dür, *Quantum* **2017**, *1*, 27.
[30] J. F. Haase, A. Smirne, J. Kołodyński, R. Demkowicz-Dobrzański, S. F. Huelga, *Quantum Meas. Quantum Metrol.* **2018**, *5*, 13.
[31] N. Friis, D. Orsucci, M. Skotiniotis, P. Sekatski, V. Dunjko, H. J. Briegel, W. Dür, *New J. Phys.* **2017**, *19*, 063044.
[32] J. Jeske, J. H. Cole, S. F. Huelga, *New J. Phys.* **2014**, *16*, 073039.
[33] R. Demkowicz-Dobrzański, J. Czajkowski, P. Sekatski, *Phys. Rev. X* **2017**, *7*, 041009.
[34] F. Reiter, A. S. Sørensen, P. Zoller, C. A. Muschik, *Nat. Commun.* **2017**, *8*, 1822.
[35] S. Lloyd, *Science* **2008**, *321*, 5895.
[36] S. Tan, B. I. Erkmen, V. Giovannetti, S. Guha, S. Lloyd, L. Maccone, S. Pirandola, J. H. Shapiro, *Phys. Rev. Lett.* **2008**, *101*, 253601.
[37] S. Guha, B. I. Erkmen, *Phys. Rev. A* **2009**, *80*, 052310.
[38] J. H. Shapiro, *IEEE Aerosp. Electron. Syst. Mag.* **2020**, *35*, 8.
[39] S. Ray, J. Schneeloch, C. C. Tison, P. M. Alsing, *Phys. Rev. A* **2019**, *100*, 012327.
[40] S. Barzanjeh, S. Guha, C. Weedbrook, D. Vitali, J. H. Shapiro, S. Pirandola, *Phys. Rev. Lett.* **2015**, *114*, 080503.
[41] S. Barzanjeh, S. Pirandola, D. Vitali, J. M. Fink, *Sci. Adv.* **2020**, *6*, 19.
[42] G. De Palma, J. Borregaard, *Phys. Rev. A* **2018**, *98*, 012101.
[43] E. D. Lopaeva, I. R. Berchera, I. P. Degiovanni, S. Olivares, G. Brida, M. Genovese, *Phys. Rev. Lett.* **2013**, *110*, 153603.
[44] T. Gregory, P.-A. Moreau, E. Toninelli, M. J. Padgett, *Sci. Adv.* **2020**, *6*, eaay2652.
[45] Q. Cai, J. Liao, B. Shen, G. Guo, Q. Zhou, *Phys. Rev. A* **2021**, *103*, 052419.
[46] M. Lanzagorta, J. Uhlmann, *Quantum Radar*, Morgan and Claypool, San Rafael, CA **2012**, p. 66.
[47] L. Maccone, C. Ren, *Phys. Rev. Lett.* **2020**, *124*, 200503.
[48] Q. Zhuang, *Phys. Rev. Lett.* **2021**, *126*, 240501.
[49] M. Sanz, U. Las Heras, J. J. García-Ripoll, E. Solano, R. Di Candia, *Phys. Rev. Lett.* **2017**, *118*, 070803.
[50] A. Holevo, *Probabilistic and Statistical Aspects of Quantum Theory*, Springer, Berlin **2011**.
[51] C. W. Helstrom, *J. Stat. Phys.* **1969**, *1*, 231.
[52] S. L. Braunstein, C. M. Caves, *Phys. Rev. Lett.* **1994**, *72*, 3439.
[53] M. G. A. Paris, *Int. J. Quantum Inf.* **2009**, *07*, 125.
[54] M. G. A. Paris, J. Rehacek, *Quantum State Estimation*, Springer-Verlag, Berlin **2004**.
[55] In a multiparameter scenario the quantum Fisher information is actually a matrix.
[56] A. Ferraro, S. Olivares, M. G. A. Paris, *arXiv:quant-ph/0503237*, **2005**.
[57] G. Adesso, S. Ragy, A. R. Lee, *Open Syst. Inf. Dyn.* **2014**, *21*, 1440001.
[58] S. Olivares, *Eur. Phys. J. Spec. Top.* **2012**, *203*, 3.
[59] A. Serafini, *Quantum Continuous Variables: A Primer of Theoretical Methods*, CRC Press, Boca Raton, FL **2017**.
[60] D. Šafránek, *J. Phys. A: Math. Theor.* **2018**, *52*, 035304.
[61] D. Šafránek, A. R. Lee, I. Fuentes, *New J. Phys.* **2015**, *17*, 073016.
[62] O. Pinel, J. Fade, D. Braun, P. Jian, N. Treps, C. Fabre, *Phys. Rev. A* **2012**, *85*, 010101.
[63] N. Friis, M. Skotiniotis, I. Fuentes, W. Dür, *Phys. Rev. A* **2015**, *92*, 022106.
[64] O. Pinel, P. Jian, N. Treps, C. Fabre, D. Braun, *Phys. Rev. A* **2013**, *88*, 040102(R).
[65] A. Monras, *arXiv:1303.3682*, **2013**.
[66] Z. Jiang, *Phys. Rev. A* **2013**, *89*, 032128.
[67] P. Marian, T. A. Marian, *Phys. Rev. A* **2016**, *93*, 052330.
[68] Y. Gao, H. Lee, *Eur. Phys. J. D* **2014**, *68*, 347.
[69] R. Nichols, P. Liuzzo-Scorpo, P. A. Knott, G. Adesso, *Phys. Rev. A* **2018**, *98*, 012114.
[70] L. Banchi, S. L. Braunstein, S. Pirandola, *Phys. Rev. Lett.* **2015**, *115*, 260501.
[71] M. Sanz, K. G. Fedorov, F. Deppe, E. Solano, in *2018 IEEE Conf. on Antenna Measurements and Applications(CAMA)*, IEEE, Piscataway, NJ **2018**, pp. 1–4.
[72] The 'quantum optics' convention takes $\kappa_1 = 1$.
[73] D. B. Arvind, N. Mukunda, R. Simon, *Pramana* **1995**, *45*, 471.
[74] R. Simon, V. Srinivasan, S. K. Chaturvedi, *J. Math. Phys.* **1998**, *40*, 7.
[75] J. Williamson, *Am. J. Math.* **1936**, *58*, 141.
[76] S. Personick, *IEEE Trans. Inf. Theory* **1971**, *17*, 240.
[77] M. Jarzyna, R. Demkowicz-Dobrzański, *New J. Phys.* **2015**, *17*, 013010.
[78] W. Górecki, R. Demkowicz-Dobrzański, H. M. Wiseman, D. W. Berry, *Phys. Rev. Lett.* **2020**, *124*, 030501.
[79] S. Morelli, A. Usui, E. Agudelo, N, Friis, *Quantum Sci. Technol.* **2021**, *6*, 025018.

[80] J. Rubio, P. Knott, J. Dunningham, *J. Phys. Commun.* **2018**, *2*, 015027.
[81] J. Rubio, J. Dunningham, *New J. Phys.* **2019**, *21*, 043037.
[82] J. Rubio, J. Dunningham, *Phys. Rev. A* **2020**, *101*, 032114.
[83] S. Kay, *Fundamentals of Statistical Signal Processing: Estimation Theory*, Prentice Hall, Hoboken, NJ **1993**.
[84] R. Demkowicz-Dobrzański, M. Jarzyna, J. Kołodyński, *Progress in Optics* **2015**, *60*, 345.
[85] H. Cramér, *Mathematical Methods of Statistics*, Vol. *43*, Princeton University Press, Princeton, NJ **1999**.
[86] C. R. Rao, in *Breakthroughs in Statistics*, Springer, Berlin **1992**, pp. 235–247.
[87] C. Eichler, D. Bozyigit, C. Lang, M. Baur, L. Steffen, J. M. Fink, S. Filipp, A. Wallraff, *Phys. Rev. Lett.* **2011**, *107*, 113601.
[88] E. Flurin, N. Roch, F. Mallet, M. H. Devoret, B. Huard, *Phys. Rev. Lett.* **2012**, *109*, 183901.
[89] S. L. Braunstein, P. van Loock, *Rev. Mod. Phys.* **2005**, *77*, 513.
[90] M. Casariego, E. Z. Cruzeiro, S. Gheradini, T. Gonzalez-Raya, R. André, G. Frazão, G. Catto, M. Möttönen, D. Datta, K. Viisanen, J. Govenius, M. Prunnila, K. Tuominen, M. Reichert, M. Renger, K. G. Fedorov, F. Deppe, H. van der Vliet, A. J. Matthews, Y. Fernández, R. Assouly, R. Dassonneville, B. Huard, M. Sanz, Y. Omar, *arXiv:2205.11424 [quant-ph]*, **2022**.
[91] T. Gonzalez-Raya, M. Casariego, F. Fesquet, M. Renger, V. Salari, M. Möttönen, Y. Omar, F. Deppe, K. G. Fedorov, M. Sanz, *arXiv:2203.07295 [quant-ph]*, **2022**.
[92] J. Oz-Vogt, A. Mann, M. Revzen, *J. Mod. Opt.* **1991**, *38*, 2339.
[93] U. Las Heras, R. Di Candia, K. G. Fedorov, F. Deppe, M. Sanz, E. Solano, *Sci. Rep.* **2017**, *7*, 9333.
[94] Note that N_S is defined as the expected photon number in a *single* mode, meaning that the actual photon number in the signal is $2N_S$.
[95] K. G. Fedorov, S. Pogorzalek, U. Las Heras, M. Sanz, P. Yard, P. Eder, M. Fischer, J. Goetz, E. Xie, K. Inomata, Y. Nakamura, R. Di Candia, E. Solano, A. Marx, F. Deppe, R. Gross, *Sci. Rep.* **2018**, *8*, 6416.
[96] In a state language this translates to the total unitary being the tensor product of two beam splitters: $U_T(\eta_1, \eta_2) = U(\eta_1) \otimes U(\eta_2)$, with $U(\eta_i) \equiv \exp[\arcsin\sqrt{\eta(\omega_i)}(\hat{s}_i^\dagger \hat{b}_i - \hat{s}_i \hat{b}_i^\dagger)]$.
[97] M. G. A. Paris, *Phys. Lett. A* **1996**, *217*, 78.
[98] R. Dassonneville, R. Assouly, T. Peronnin, P. Rouchon, B. Huard, *Phys. Rev. Appl.* **2020**, *14*, 044022.
[99] K. G. Fedorov, L. Zhong, S. Pogorzalek, P. Eder, M. Fischer, J. Goetz, E. Xie, F. Wulschner, K. Inomata, T. Yamamoto, Y. Nakamura, R. Di Candia, U. Las Heras, M. Sanz, E. Solano, E. P. Menzel, F. Deppe, A. Marx, R. Gross, *Phys. Rev. Lett.* **2016**, *117*, 020502.
[100] T. González-Raya, M. Sanz, *Quantum* **2022**, *6*, 783.
[101] J. Zhang, T. Li, R. Kokkoniemi, C. Yan, W. Liu, M. Partanen, K. Y. Tan, M. He, L. Ji, L. Grönberg, M. Möttönen, arXiv:2003.01356, **2020**.
[102] C. Munuera-Javaloy, I. Arrazola, E. Solano, J. Casanova, *Phys. Rev. B* **2020**, *101*, 104411.
[103] S. Dambach, B. Kubala, J. Ankerhold, *New J. Phys.* **2017**, *19*, 023027.
[104] C. K. Law, I. A. Walmsley, J. H. Eberly, *Phys. Rev. Lett.* **2000**, *84*, 5304.